GeMS/GSAOI performances from a user perspective

Dalessandro, Emanuele, Saracino, Sara, Origlia, Livia, Marchetti, Enrico, Ferraro, Francesco, et al.

Emanuele Dalessandro, Sara Saracino, Livia Origlia, Enrico Marchetti, Francesco R. Ferraro, Barbara Lanzoni, Douglas Geisler, Francesco Mauro, "GeMS/GSAOI performances from a user perspective," Proc. SPIE 9909, Adaptive Optics Systems V, 99095V (27 July 2016); doi: 10.1117/12.2230978

SPIE.

Event: SPIE Astronomical Telescopes + Instrumentation, 2016, Edinburgh, United Kingdom

GEMS/GSAOI PERFORMANCES FROM A USER PERSPECTIVE

Emanuele Dalessandro[a,b], Sara Saracino[a,b], Livia Origlia[b], Enrico Marchetti[c], Francesco R. Ferraro[a], Barbara Lanzoni[a], Douglas Geisler[d], and Francesco Mauro[d,e]

[a]University of Bologna, Physics & Astronomy Dept., Viale Berti Pichat 6-2, I-40127 Bologna, Italy
[b]INAF - Osservatorio Astronomico di Bologna, Via Ranzani 1, I-40127 Bologna, Italy
[c]ESO - European Southern Observatory, Karl Schwarzschild Str. 2, D-85748 Garching bei Muenchen, Germany
[d]Departamento de Astronomía, Universidad de Concepción, Casilla 160-C, Concepción, Chile
[e]Millennium Institute of Astrophysics, Chile

ABSTRACT

Ground-based near-IR imagers assisted by Multi Conjugate Adaptive Optics (MCAO) systems are the technological frontier to obtain high-quality stellar photometry in crowded fields at the highest possible spatial resolution. The Gemini MCAO System (GeMS) feeding the Gemini South Adaptive Optics Imager (GSAOI) is the only facility of this kind currently available to the Community. We used a set of images obtained in the J and K_s bands of the central regions of two Galactic bulge globular clusters (Liller 1 and NGC 6624) with GeMS/GSAOI, under significantly different atmospheric conditions. We characterized the performances of the system in terms of efficiency and uniformity of the Point Spread Function (PSF) over the field of view with varying seeing, airmass and tip-tilt star asterisms. We also compared the PSF performances of GeMS/GSAOI with the HST/ACS ones in the F606W and F814W bands.

Keywords: Adaptive Optics; Infrared Imaging; Point Spread Functions; Stellar Photometry; Globular Clusters

1. INTRODUCTION

The first MCAO system used for nighttime astronomical observations was the Multi-Conjugate Adaptive-optics Demonstrator (MAD) operating at the VLT in 2007-2008 (Marchetti et al. 2007). MAD used up to three natural guide stars for the wavefront sensing and tip-tilt correction and two deformable mirrors conjugated at the ground and at an altitude of 8.5 Km, providing a corrected field of view of about $1' \times 1'$. A few works on stellar photometry in the dense stellar fields of Galactic globular clusters (GCs) (see, e.g., Ortolani et al. 2008; Ferraro et al. 2009; Moretti et al. 2009; Bono et al. 2010) have shown how effective a MCAO system like MAD could be in providing uniform Point Spread Functions (PSF) and accurate photometry across the entire $1' \times 1'$ field of view.

Since 2013, the Gemini Multi-Conjugate adaptive optics System (GeMS) together with the Gemini South Adaptive Optics Imager (GSAOI) at the Gemini South telescope (Rigaut et al. 2014; Neichel et al. 2014a) is regularly offered to the Community for observations. This is the only MCAO facility currently at work. GeMS is the first sodium based multi-laser MCAO system. It uses five lasers and three tip-tilt stars to provide an efficient correction over a $2' \times 2'$ field of view. GSAOI is a NIR imager equipped with four 2k×2k detectors with 20 mas pixel size, covering a 85" × 85" field of view, designed to work at the diffraction limit of an 8m telescope.

Further author information: (Send correspondence to Emanuele Dalessandro): E-mail: emanuele.dalessandr2@unibo.it, Telephone: +39 051 2095705

Adaptive Optics Systems V, edited by Enrico Marchetti, Laird M. Close, Jean-Pierre Véran, Proc. of SPIE Vol. 9909, 99095V
 · doi: 10.1117/12.2230978

The proper characterization of the image quality delivered by the GeMS/GSAOI system and of the parameters that mostly contribute to set its overall efficiency is extremely important to decide the best observational strategy and to maximize the scientific output. It also provides useful information for the future generation of MCAO systems at the 30-40m class giant telescopes.

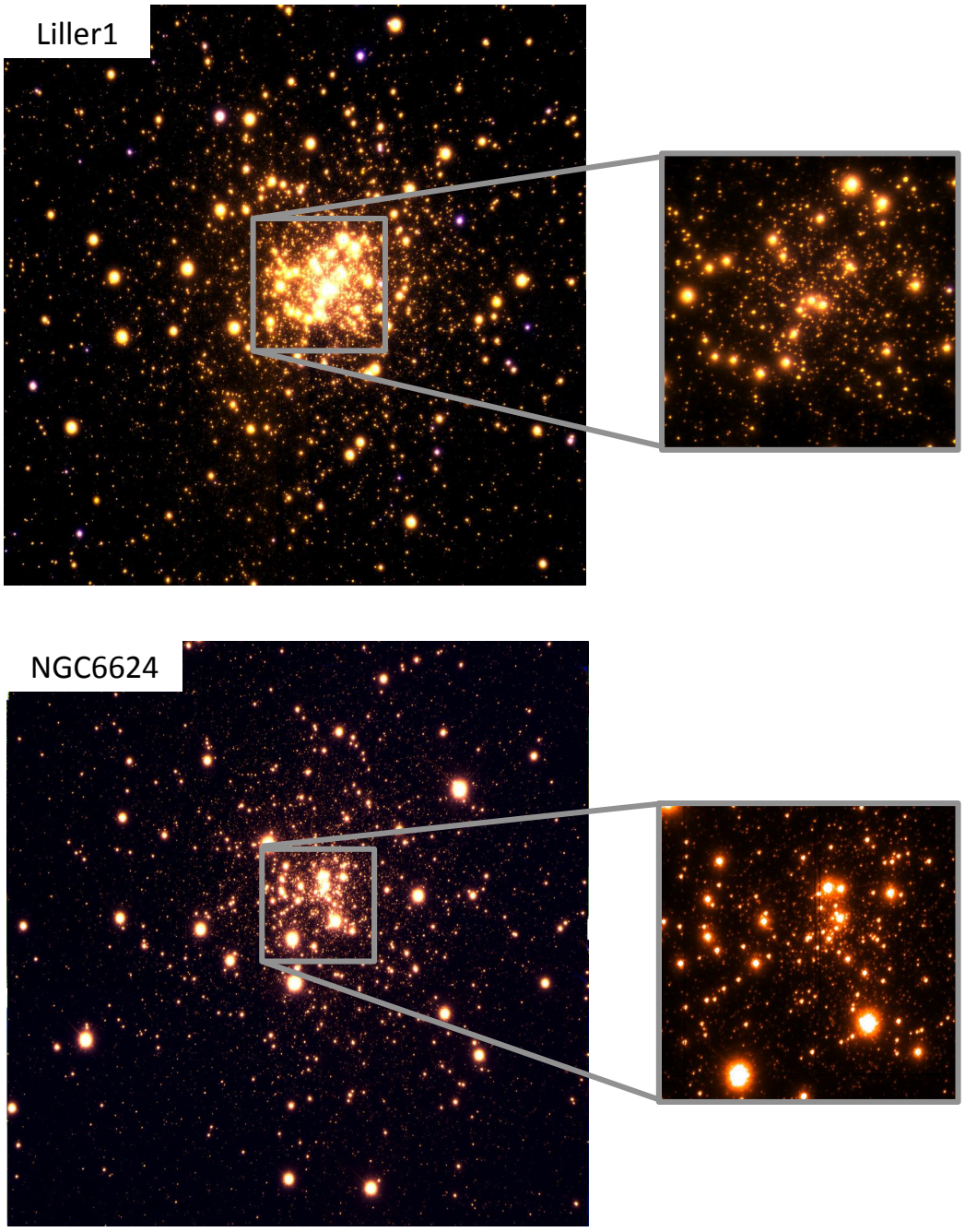

Figure 1. The spectacular images of Liller1 and NGC 6624 obtained with GeMS@GEMINI. These false-color mosaiced images (with a total size of $\sim 95" \times 95"$) have been obtained by combining a 2×2 array of dithered frames acquired in the NIR J and K_s pass-bands. A zoom of the core regions ($\sim 15" \times 15"$) is shown in the insets.

2. DATA-SET AND OBSERVING CONDITIONS

By using GeMS/GSAOI we observed the central regions of two Galactic bulge GCs, namely Liller 1 and NGC 6624, between April 2013 and May 2013. Two different sets of images for Liller 1 (3 in J and 10 in K_s on April 2013, 9 in J and 5 in K_s on May 2013) and one set for NGC 6624 (13 in J and 14 in K_s on May 2013) have been acquired, using an integration time of 30 sec for each exposure.

Each image has been sky-subtracted and flat-field corrected using suitable master sky and dome flat frames in the J and K_s bands (see Saracino et al. 2015 for further details).

Table 1. Selected tip-tilt guide stars.

STAR	Ks	H	J	I	V	R	fmag
Liller 1							
NGS 1 (2MASS J17332197-3323043)	12.799	12.715	12.958	–	–	–	15.338
NGS 2 (2MASS J17332484-3322502)	11.127	11.185	11.418	–	–	–	13.947
NGS 3 (2MASS J17332609-3323129)	11.297	11.074	11.735	–	–	–	13.577
NGC 6624							
NGS 1 (2MASS J18233752-3022018)	8.472	8.723	9.730	11.3850	13.4520	13.094	13.793
NGS 2 (2MASS J18234108-3022221)	8.987	9.202	10.100	11.6230	12.9890	13.219	13.662
NGS 3 (2MASS J18234052-3021392)	8.827	9.274	9.899	12.8800	14.1040	13.776	10.889 (blend)

Three reference guide stars for each cluster (see Table 1) for the tip-tilt correction have been selected. The guide stars of NGC 6624 are luminous and cool giants near the tip, likely cluster members, with $fmag \sim R \sim$13-14. The guide stars in Liller 1 are blue foreground stars, with significantly fainter J, H, K_s magnitudes and similar R-band magnitudes compared to those of NGC 6624, with the exception of NGS 1, which is a couple of magnitude fainter. Since the R-band is the spectral range where the wavefront is mostly sensed, this may have some relevance in the final performances (see Section 3.2).

The mosaiced two color images of Liller 1 and NGC 6624, obtained by combining all the images available are shown in Figure 1. We recall that each image is actually the mosaic of four chips that have been calibrated independently.

The data of NGC 6624 have been obtained with an average seeing at $500nm$ of $\sim$ 0.65", while those for Liller 1 have been obtained under significantly worse conditions with $\sim$ 1.25".

The atmospheric seeing at the observed airmass has been computed using the following formula: $s(500nm, z) = 10.31/(R_0(500nm) \times secz^{-3/5})$, where R_0 is the Fried parameter at $\lambda = 500nm$ and at the zenith, as reported in each image header.

3. POINT SPREAD FUNCTION CHARACTERIZATION

We used the IDL-based Multi-Strehl Meter software written by Marchetti et al. (2006) to analyze the stellar PSF in the science images and measure its Full Width at Half Maximum (FWHM), Strehl ratio (SR) and Encircled Energy (EE) with varying observing conditions, in order to characterize the performances of the adaptive optics system.

Typically about 200 isolated and bright stars homogeneously distributed in the field of view in each image have been selected and their FWHM, SR and EE have been measured. The EE has been computed within a circular aperture of two times the measured FWHM, i.e. the typical aperture adopted in the photometric analysis. For each quantity we computed the average and corresponding dispersion values in each image and analyzed their trend as a function of the observing conditions.

3.1 PSF spatial mapping

Liller 1 images in the K_s band have been obtained with seeing between 0.9" and 1.6", while J-band images in slightly better observing conditions, with seeing ranging from 0.7" to 1.2".

In Figure 2 we show the maps of the FWHM and SR for the images acquired under the best seeing conditions in both the K_s and J bands. As expected, better performances are obtained in the surrounding of the guide star asterism, where AO corrections are more efficient, thus yielding smaller values of FWHM and higher values of the SR. In particular, in the K_s band image (seeing=0.92"), the FWHM has a minimum value of ~ 75 mas, which is very close to the diffraction limit, while in the $J-$band image (seeing=0.72") a minimum FWHM~ 50 mas is reached. SR up to $\sim 60\%$ in K_s and $\sim 25\%$ in J images have been measured.

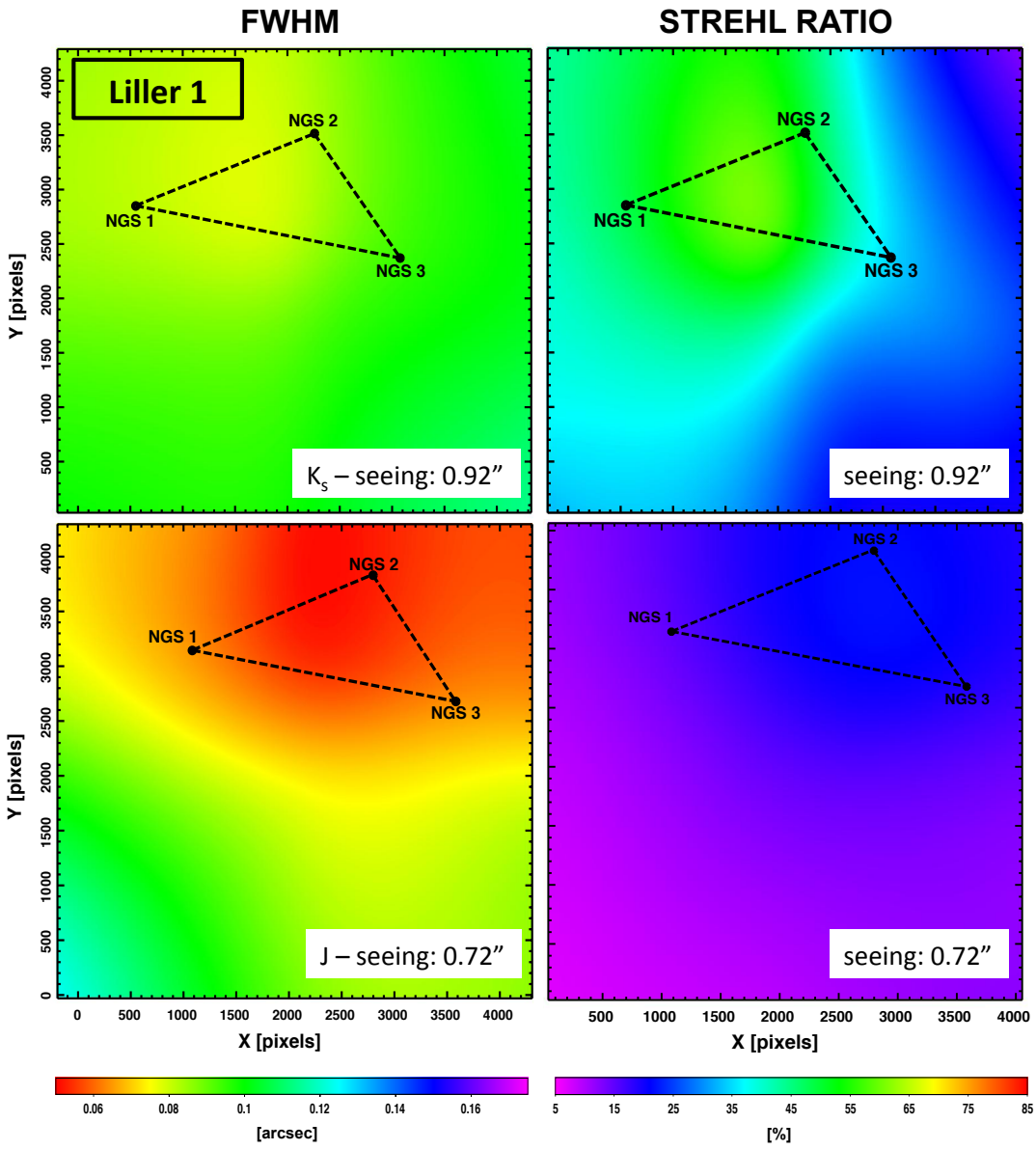

Figure 2. FWHM (left panels) and SR (right panels) maps for the best-seeing K_s (top panels) and J (bottom panels) images of Liller 1. The triangle indicates the guide star asterism. The quoted seeing values are at $500nm$. Color coding from magenta (worst) to red (best) is a performance indicator.

All images obtained for NGC 6624 have been acquired in very good seeing conditions, in a relatively narrow range between 0.5" and 0.9". In Figure 3 we show the FWHM and SR maps for the K_s and J bands. The color coding is the same of Figure 2, for a direct comparison. As in the case of Liller 1, GeMS/GSAIO delivers better performances (i.e. smaller FWHM and higher SR) in the surrounding of the guide star asterism. Similar maximum FWHM and minimum SR values to those in Liller 1 are obtained. However, the better seeing conditions during the observation of NGC 6624 provides more uniform and better SR over a larger fraction of the field of view compared to Liller 1.

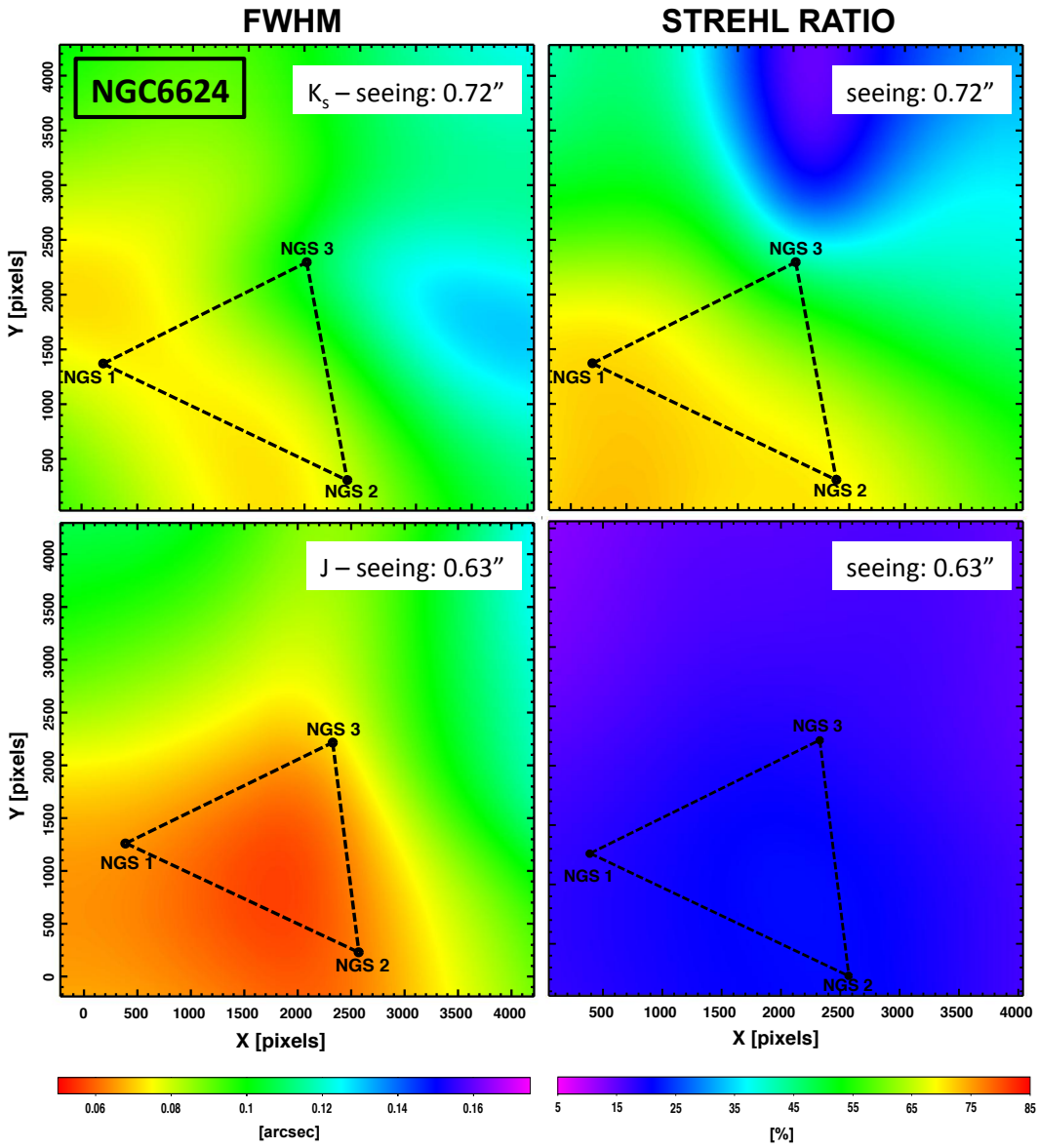

Figure 3. FWHM (left panels) and SR (right panels) maps for two K_s (top panels) and J (bottom panels) images of NGC 6624. The triangle indicates the guide star asterism. The quoted seeing values are at $500nm$. The color scale is the same as in Figure 2 (magenta worst and red best) to allow a direct comparison.

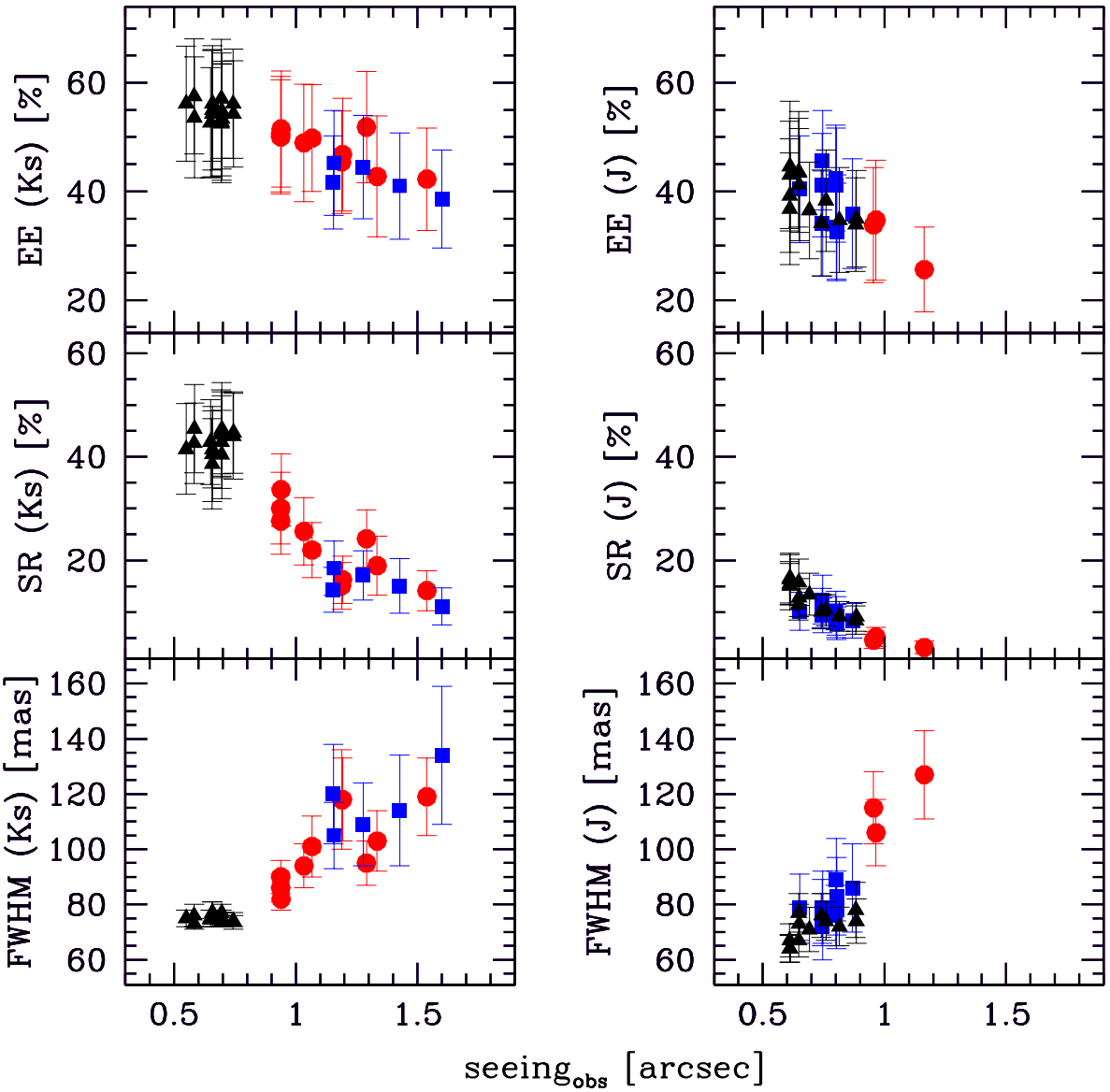

Figure 4. Average FWHM, SR and EE values with varying the seeing at 500nm at the observing airmass. Left panels: measurements in the K_s-band, right panels: measurements in the J-band. Triangle refer to measurements of stars in NGC 6624, circles and squares refer to measurements of stars in Liller 1 as observed in two different nights, respectively.

3.2 PSF average properties

For a more quantitative analysis we studied how the average FWHM, SR and EE values change as a function of the observed seeing.

The left panels of Figure 4 show the average FWHM, SR and EE in the K_s band as a function of the observed seeing. At observed seeing < 0.8", constant, average FWHMs very close to the diffraction limit of 70 mas, SR of $\sim 40\%$ and EE of 55% have been measured in the NGC 6624 images (black triangles). Liller 1 images (blue and red symbols), observed with worse seeing condition between 0.9" and 1.6", give average values of FWHM between 80 and 140 mas, SR between 30% and 10% and EE between 50% and 40%.

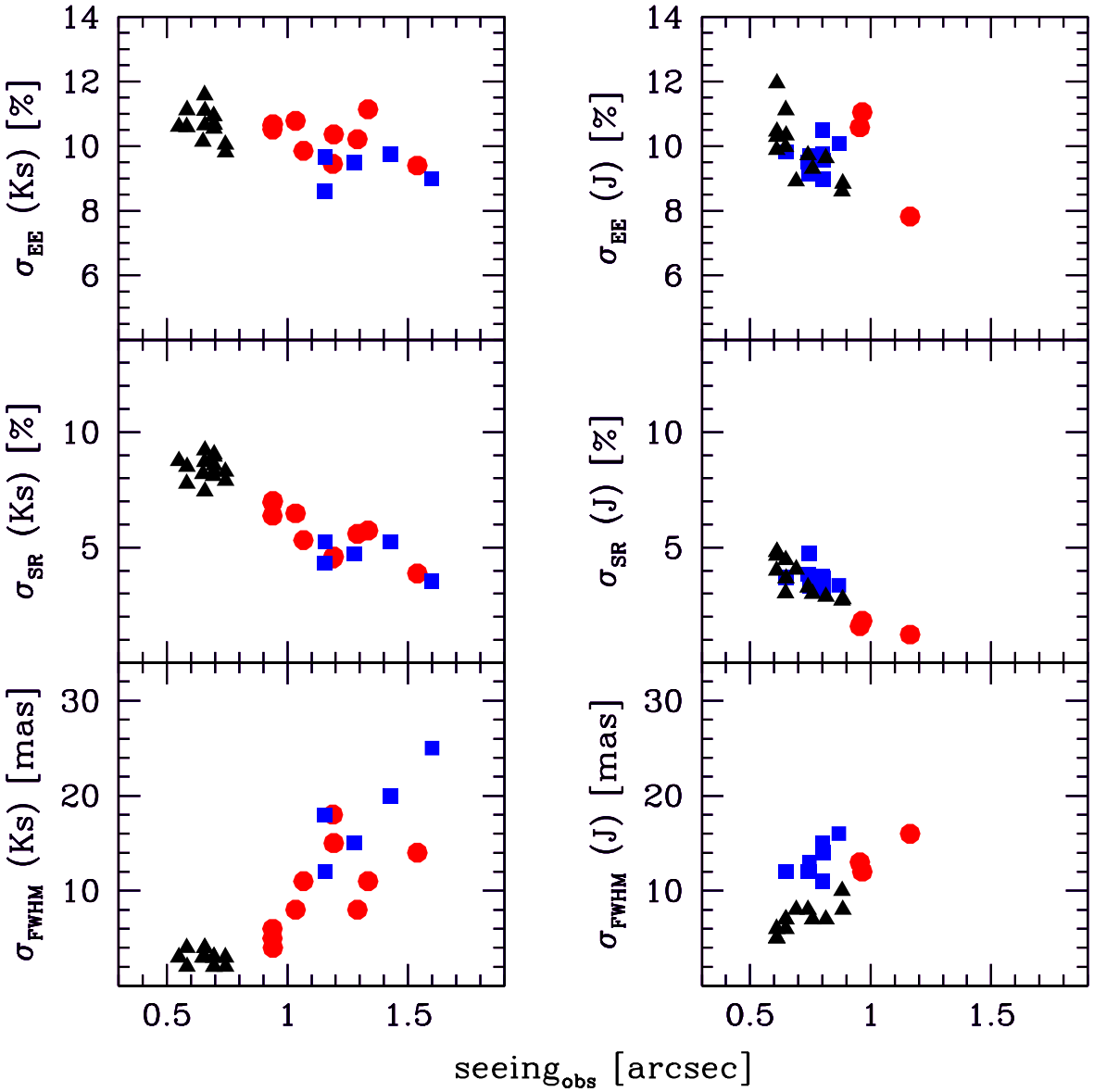

Figure 5. Dispersion around the average FWHM, SR and EE values with varying the seeing at 500nm at the observing airmass. Left panels: measurements in the K_s-band, right panels: measurements in the J-band. Triangle refer to measurements of stars in NGC 6624, circles and squares refer to measurements of stars in Liller 1 as observed in two different nights, respectively (see Table 1).

The right panels of Figure 4 show the corresponding average values measured in J band images. For seeing varying between 0.6" and 1.2", average FWHMs between 60 and 120 mas, SR between ∼15% and a few percent and EE between 40% and 20% have been measured.

The smoother variation of the EE with seeing is somewhat expected, given that it is computed within a variable aperture, proportional to the variable FWHM, and it indicates that the seeing primarily impacts the spatial resolution (i.e. the FWHM and the SR) and to a lower extent the photometric signal (i.e. the EE), when computed via variable PSF fitting.

A sub-sample of images in the J-band of Liller 1 and NGC 6624 have been acquired with the same seeing, between 0.6" and 0.9" and can be used to check the impact of the different asterisms of the two clusters, and in particular the fact that one guide star in Liller 1 has a significantly fainter R-band magnitude (see Table 1). On average, the Liller 1 images show a $\sim 10-15\%$ larger FWHM, that could be indeed a consequence of the significantly fainter guide star.

While the average values of the FWHM, SR and EE are an indication of the system efficiency, their dispersion provides a quantitative estimate of the uniformity of the PSF across the field of view. Modeling the PSF variations within the FOV is indeed one of the major issue in the photometric analysis of AO-assisted images. In the following we quantify this effect in our data-set as a function of the observing conditions.

As shown in Figure 5, the dispersion around the average FWHM increases for increasing seeing in a similar fashion as the FWHM itself (Figure 4). This indicates that a bad seeing worsens both the spatial resolution and its uniformity over the field of view. At variance, the dispersion around the average SR and EE decreases with increasing seeing.

A more uniform SR and EE across the field of view with worsening seeing conditions is somewhat expected. Indeed, at variance with the FWHM, the SR and the EE are quantities somewhat normalized to the seeing contribution. Hence, when the seeing worsen, its contribution progressively dominates over the diffraction limit peak, and being almost constant across the field of view, provides a progressively less efficient but more uniform PSF.

4. GEMS/GSAOI *VS* HST/ACS PERFORMANCES

In verifying the potentiality of ground-based MCAO-assisted imagers to obtain accurate photometry in dense stellar fields, it is very meaningful to compare the performance of the GeMS/GSAOI system with the Hubble Space Telescope (HST) imagers. A comparison between a GeMS/GSAOI J-band and the HST F814W images is shown in Figure 6.

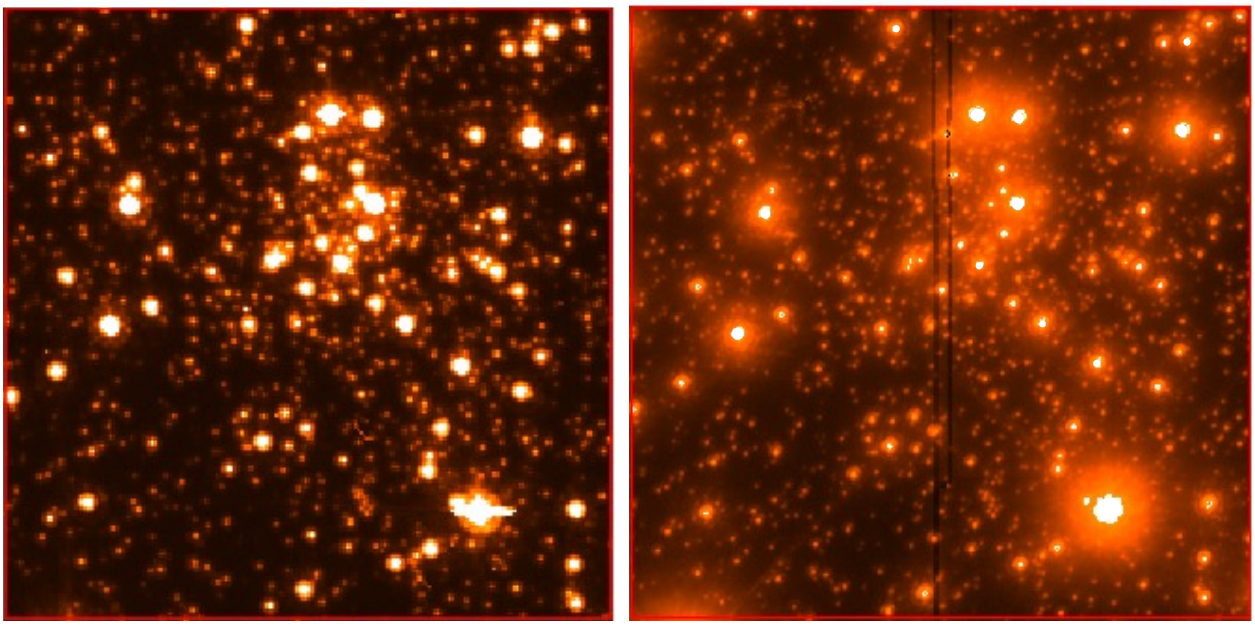

Figure 6. A 10" $\times$ 10" region of NGC 6624 as seen from the ACS/WFC in the F814W band (left panel) and from GeMS/GSAOI in the J band (right panel).

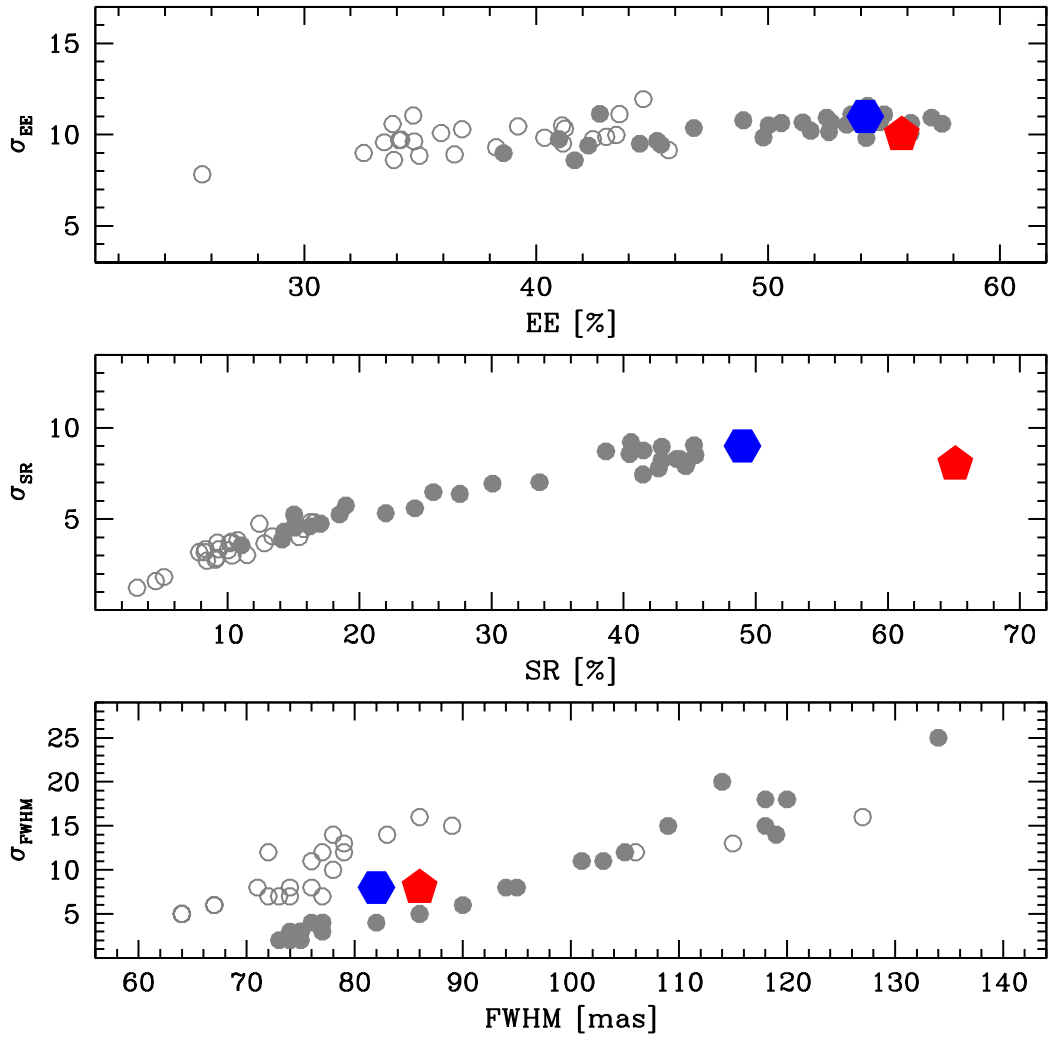

Figure 7. Dispersion around the average FWHM, SR and EE values as a function of the corresponding average values, as computed in the GeMS/GSAOI J (open circles) and in the K_s (filled circles) images, and in the ACS/HST F606W (hexagon) and F814W (pentagon) ones.

We used two short exposures ($t_{exp} = 15$ sec) of NGC 6624 taken with ACS/WFC in the F606W and F814W bands (Prop: 10775; PI: Sarajedini) and we selected about 200 high signal-to-noise and isolated stars to compute average FWHM, SR and EE and their dispersions around the mean, by performing the same analysis as for GeMS/GSAOI images.

We obtain average values of FWHM of 82 mas and 86 mas for the F606W and F814W respectively. While the average FWHM for the F814W is consistent with the nominal diffraction limit of HST at these wavelength (∼85 mas), the FWHM in the F606W is significantly larger (by $\sim 30\%$) than the nominal diffraction limit (∼63 mas), but this is somewhat expected, since at these wavelengths the limiting factor is the undersampling of the PSF. We find also that the overall variation of the FWHM along the entire ACS FOV ($\sim 200'' \times 200''$) is $\sim 8\%$. This value is consistent with a $\pm 10\%$ variation estimated by using a significantly larger data-set by Anderson & King (2006). For the same stars we estimated $SR \sim 50\%$ and $\sim 65\%$ for the F606W and F814W, respectively, and $\sigma_{SR} < 10\%$ for both filters. Moreover we find $EE \sim 55\%$ and $\sigma_{EE} \sim 10\%$ for both filters.

These latter values are consistent with those estimated by Sirianni et al. (2005; Table 3) within a comparable aperture of 2×FWHM (corresponding to an equivalent circular radius between 50 and 100 mas) for white dwarfs spectro-photometric standards located at the center of the two ACS/WFC chips.

In Figure 7 we plot the dispersion around the average FWHM, SR and EE values as a function of the corresponding average values for the GeMS/GSAOI J and K_s images, as well as for the ACS/HST F606W and F814W ones. For sub-arcsec seeing conditions, GeMS/GSAIO delivers images with comparable or even better PSF FWHMs than ACS and also similar uniformity over the field of view (at least in the K_s-band). At variance, the Strehl ratios and the EE are on average significantly lower than the corresponding values of ACS, while their variation over the field of view is comparable (around 10%). EE>50% as for ACS have been measured only in K_s images with sub-arsec seeing.

5. CONCLUSIONS

The analysis performed on the GeMS/GSAOI J and K_s images of the central region of two GCs have provided very interesting results on the PSF performances.

A diffraction limit PSF FWHM (∼80 mas), SR≥ 40% and EE ≥ 50% with a dispersion around 10% over the 85"×85" field of view can be obtained only in the K_s band and for sub-arcsec seeing at the observed airmass.

In the same good seeing conditions FWHMs between 60 and 80 mas, SR>10% and EE ≥40% can be obtained in the J band.

For seeing at the observed airmass exceeding 1", the performances worsen but it is still possible to perform PSF fitting photometry with $\sim 25\%$ EE efficiency in J and $\sim 40\%$ in K_s bands.

When compared to the performances available from HST-ACS, GeMS/GSAOI can provide slightly better spatial resolution, thus allowing a better sampling of the innermost, densest core region, but a lower efficiency/sensitivity, as traced by the SR and EE values. Both instruments can guarantee an uniform PSF (at a level of $10-15\%$ or better) over their entire field of view.

ACKNOWLEDGMENTS

E.D and S.S. acknowledges support from the *Cosmic-Lab* project funded by the European Research Council under contract ERC-2010-AdF-267675. L.O. acknowledges the PRIN-INAF 2014 CRA 1.05.01.94.11: "Probing the internal dynamics of globular clusters. The first comprehensive radial mapping of individual star kinematics with the new generation of multi-object spectrographs" (PI: L. Origlia).

REFERENCES

Anderson, J., & King, I. R. 2006, Instrument Science Report ACS 2006-01, 34 pages
Bono, G., et al. 2010, ApJ, 798, 74
Ferraro, F. R., et al. 2009, Nature, 462, 483
Marchetti, E., Brast, R., Delabre, B., et al. 2006, SPIE, 6272, 62720O
Marchetti, E., et al., 2007, The Messenger 129, 8
Moretti, A., et al. 2009, A&A, 493, 539
Neichel, B., Lu, J. R., Rigaut, F., Ammons, S. M., Carrasco, E. R., Lassalle, E. 2014, MNRAS, 445, 500
Ortolani, S., et al. 2008, ApJ, 737, 31
Rigaut, F., et al. 2014, MNRAS, 437, 2361
Saracino, S., Dalessandro, E., Ferraro, F. R., et al. 2015, ApJ, 806, 152
Sirianni, M., Jee, M. J., Benítez, N., et al. 2005, PASP, 117, 1049